

Radio Imaging Spectropolarimetry of CMEs and CME Progenitors

Principal Author:

Bin Chen¹  *New Jersey Institute of Technology*

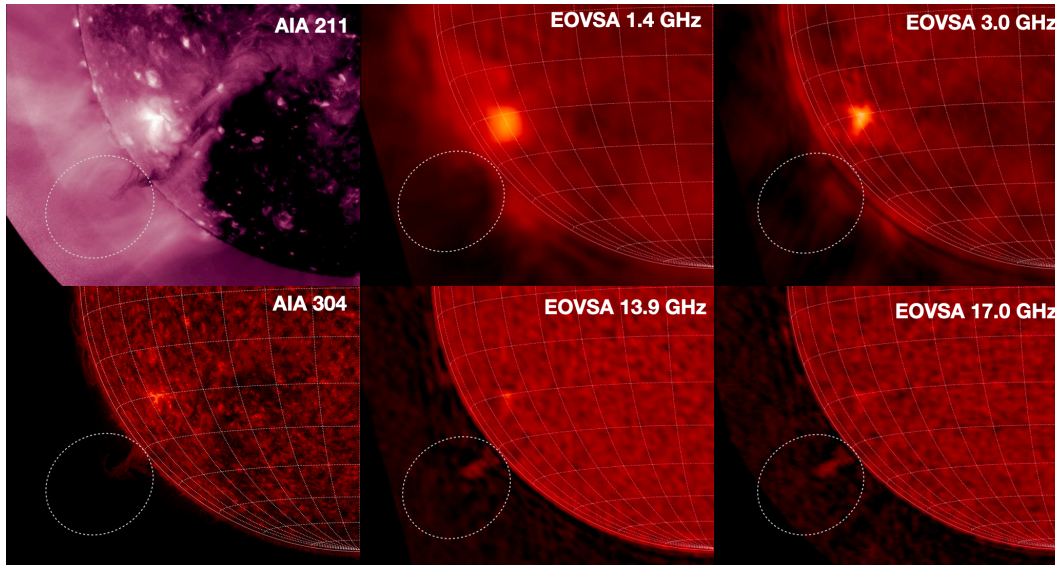
Email: binchen@njit.edu; Phone: (973) 596-3565; Web: <https://binchensun.org>

Co-authors

Timothy S. Bastian² , Sarah Gibson³ , Yuhong Fan³ , Stephen M. White⁴ , Dale E. Gary¹ , Angelos Vourlidas⁵ , Sijie Yu¹ , Surajit Mondal¹ , Gregory D. Fleishman¹ , Pascal Saint-Hilaire⁶ 

[1] New Jersey Institute of Technology; [2] National Radio Astronomy Observatory; [3] High Altitude Observatory; [4] Air Force Research Laboratory; [5] JHU Applied Physics Laboratory; [6] University of California, Berkeley

Co-Signers & Affiliations: see spreadsheet



Synopsis

Coronal mass ejections (CMEs) are the most important drivers of space weather. Central to most CMEs is thought to be the eruption of a bundle of highly twisted magnetic field lines known as magnetic flux ropes. A comprehensive understanding of CMEs and their impacts hence requires detailed observations of physical parameters that lead to the formation, destabilization, and eventual eruption of the magnetic flux ropes. Recent advances in remote-sensing observations of coronal cavities, filament channels, sigmoids, EUV “hot channels,” white light CMEs, and in situ observations of magnetic clouds points to the possibility of significant progress in understanding CMEs. In this white paper, we provide a brief overview of the potential of radio diagnostics for CMEs and CME progenitors, with a particular focus on the unique means for constraining their magnetic field and energetic electron population. Using synthetic observations based on realistic 3D MHD models, we also demonstrate the transformative potential of advancing such diagnostics by using broadband radio imaging spectropolarimetry with a high image dynamic range and high image fidelity. To achieve this goal, a solar-dedicated radio facility with such capabilities is recommended for implementation in the coming decade.

1 Introduction

Coronal mass ejections (CMEs) are violent eruptions of coronal plasma and magnetic field from the Sun, involving a few times 10^{14} to several $\times 10^{16}$ grams of the material moving into the interplanetary medium with speeds of a few hundred to more than $2,000 \text{ km s}^{-1}$. CMEs can drive significant geomagnetic storms and other space weather activity. In fact, the strongest space weather effects are usually related to the impact of CMEs with B_z anti-aligned with the Earth's magnetic field. Therefore, a detailed understanding of the formation, initiation, eruption, and evolution of CMEs and their subsequent geospace impacts is of vital importance for space weather science and applications. In addition, fast CMEs are usually accompanied by long-duration eruptive solar flares and large solar energetic particle (SEP) events. Quantitative measurements of the physical properties of CMEs constitute an essential piece to completing the "system science" of solar eruptions, and hence are of fundamental importance for solar- and helio-physics. Last but not least, the understanding of solar CMEs serves as a "stepping stone" for addressing exo-space weather in other stellar systems and the habitability of exoplanets.

To make progress in achieving a comprehensive picture, the following measurements must be obtained:

- The magnetic field configuration of the pre-eruption magnetic flux ropes and quantifying their plasma environment. This measurement is crucial in determining the formation and initiation conditions of CMEs.
- Measuring the size, mass, speed, and magnetic field of CMEs from their early eruption in the low corona to their propagation throughout the interplanetary space. These observational inputs are essential for predicting the arrival of CMEs and evaluating their geospace impacts.
- Mapping the morphology, magnetic field configuration, and plasma parameters of CME-driven shocks. This requirement is compulsory to study the origin of large SEP events, which are themselves important space weather manifestations.

Traditionally white-light coronagraph observations have been the primary means for studying CMEs. However, radio observations provide a rich variety of complementary diagnostic methods for obtaining such observational constraints. We refer interested readers to recent reviews by [Vourlidas et al. \(2020\)](#) and [Carley et al. \(2020\)](#) for more comprehensive discussions on the details of these methods and the progress made in the past two decades, as well as their complementarity to observations at other wavelengths. For a discussion of coronal cavity magnetic diagnostics at UV and optical/IR wavelengths, see the white paper by [Gibson et al. \(2022\)](#). In this white paper, we will focus on radio diagnostics for coronal cavities and erupting CMEs, with an emphasis on the uniqueness in measuring the magnetic field and energetic electrons in CMEs and CME progenitors, as well as their highly complementary nature to optical/infrared spectropolarimetry techniques. We argue that the next major advance in radio diagnostics calls for a solar-dedicated instrument that is capable of performing broadband radio dynamic imaging spectroscopy and polarimetry with a high dynamic range, high image fidelity, and high sensitivity.

2 Coronal Cavities as CME Precursors

Coronal cavities have been observed in the Sun’s corona for several decades. They are of particular interest because of their close relationship with CMEs (Gibson et al. 2006). CMEs observed in white light often show a three-part structure: a bright expanding loop followed by a dark cavity containing a bright core that corresponds to an erupting prominence. This structure is mirrored in coronal cavities observed on the solar limb where a bright loop or coronal streamer and dark cavity are seen in quiescence; a bright prominence core is also commonly seen. Seen against the solar disk, coronal cavities overlie solar filaments or, more generally magnetic polarity inversion lines. A coronal cavity is often destabilized leading to a CME and hence they can be considered as CME precursors. These ejections are magnetically driven, the energy stored in twisted or sheared magnetic fields prior to eruption.

Clearly, **a quantitative understanding of the physical attributes of coronal cavities is needed, particularly of the magnetic field topology and the magnetic free energy available.** Significant progress has been made on the temperature and density structure of coronal cavities over the past decade. For example, Reeves et al. (2012) used the X-ray telescope (XRT) on board the Hinode spacecraft to study the thermal soft X-ray emission in cavities with hot cores, showing cavity temperatures of 1.5–1.65 MK and core temperatures of 1.7–2 MK. Forward-models of data from the Hinode EUV imaging Spectrometer (EIS) and the white-light polarization brightness measured by the Mauna Loa Solar Observatory (MLSO) Mk4 coronagraph were used (Schmit & Gibson 2011) to infer the density of a cavity and the surrounding streamer from 1.05–1.25 R_{\odot} . In cavities, densities ranging from $0.5 - 3 \times 10^8 \text{ cm}^{-3}$ were found over this radial range whereas streamer densities of $0.8 - 5 \times 10^8 \text{ cm}^{-3}$ were found. For the magnetic field, recent results from the Coronal Multi-Channel Polarimeter (CoMP) show that the linearly polarized infrared (IR) emission in coronal cavities is consistent with a magnetic flux rope topology. However, **a critical missing ingredient is quantitative measurements of the vector magnetic field.**

At optical/IR wavelengths, spectropolarimetry observations have been used to constrain the plane-of-the-sky direction of the magnetic field of coronal cavities (based on the saturated Hanle effect; see, e.g., Bak-Stęślicka et al. 2013). To measure the line-of-sight (LOS) component of the field, much more sensitive spectropolarimetry measurements are necessary to detect the extremely weak Stokes-V signal due to Zeeman splitting. The expected circular polarization degree (V/I) of the off-limb measurements is only $\lesssim 0.1\%$, or 10^{-9} of the brightness at the disk center. As a result, such measurements are only possible for off-limb sources and require large-aperture coronagraphs operating at a telescope site with excellent atmospheric conditions. The Daniel K. Inouye Solar Telescope (DKIST) and the proposed COronal Solar Magnetism Observatory (COSMO) are poised to make major advances in this area (see the white paper by Tomczyk et al. 2022 for details).

At radio wavelengths, the Stokes-V signal of the coronal magnetic field via thermal free-free emission is, in fact, prominent. In the optically thin regime, the degree of circular polarization $p = V/I$ is given by $p \approx [0.56 B_{\text{LOS}}/\nu_{\text{GHz}}]\%$, where B_{LOS} is the LOS component of the magnetic field (weighted by the square of the density in the source) and ν_{GHz} is the observing frequency in GHz (Casini et al. 2017). For example, a B_{LOS} of 20 G would give rise to a polarization degree of order 10% at 1 GHz—that is, 100 times stronger than that of the optical/IR signal via Zeeman splitting! Thanks to their comparable radio brightness relative to the disk, **such B_{LOS} measurements can be made for both the coronal cavities above the limb and, uniquely, also their on-disk**

counterparts—sigmoids or filament channels. In addition, such measurements can be obtained at a time cadence of few seconds. Therefore, **the radio measurements can be used to reveal rapid dynamic evolution of the plasma structure and magnetic field configuration of CME precursors**, which is another unique diagnostic potential available to this technique.

As a demonstration, we use a realistic 3D MHD model of a magnetic-flux-rope-hosting coronal cavity developed by Fan & Liu (2019) (Fig. 1) to calculate the corresponding synthetic radio Stokes I and V emission maps at multiples frequencies using the FORWARD package (Gibson et al. 2016). An example for 1 GHz is shown in Figs. 1(e) and (f). For this model, the Stokes V/I signal at 1 GHz reaches a peak of $\sim 7\%$ in a region that coincides with the core of the flux rope (located just above the dense and cool filament) where B_{LOS} reaches a maximum. Multi-frequency mapping enables spectral analysis (panels g, h), and the spatial distribution and temporal variation of the Stokes V and I maps serve as an excellent tool to derive the spatial and temporal evolution of key physical parameters including B_{LOS} , plasma density, and temperature.

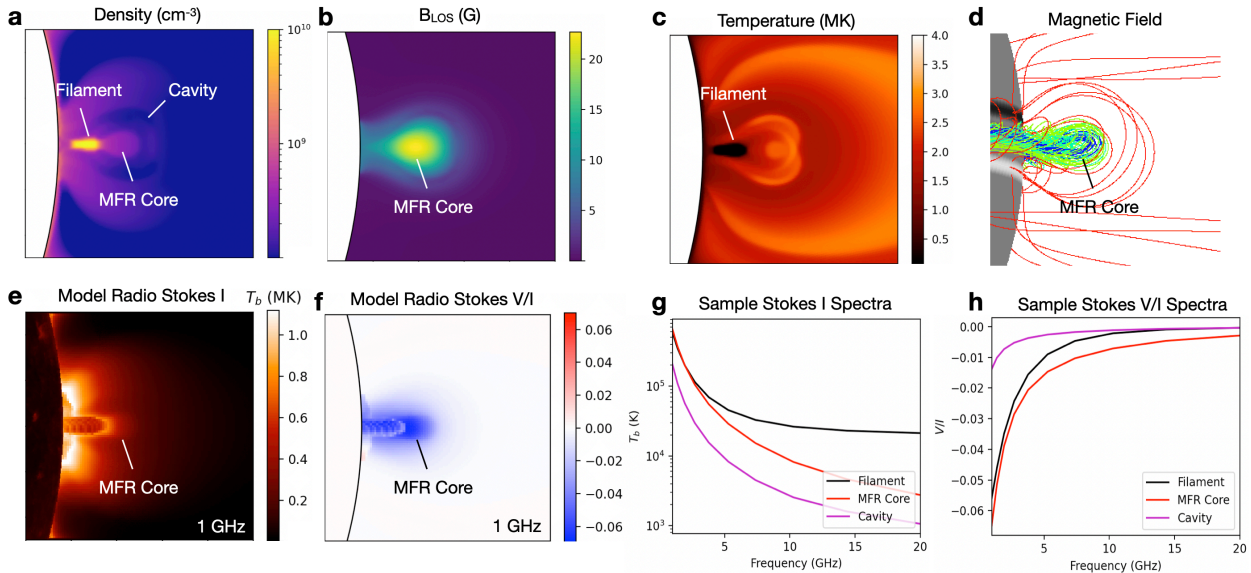


Figure 1: Radio observations can be used to derive maps of key physical parameters of coronal cavities, including their plasma density, temperature, and LOS magnetic field. (a–d): Parameters of the 3D MHD coronal cavity model (showing those at the mid-plane), which features a filament-hosting twisted magnetic flux rope viewed end on (from Fan & Liu 2019). (e) and (f): Synthetic radio thermal free-free Stokes I and V/I maps at 1 GHz calculated by applying radiative transfer to the 3D MHD model. They bear striking similarities to the density and B_{LOS} distributions in the MHD model. (g) and (h): Stokes I and V/I spectra sampled at three locations that correspond to the filament, flux rope core, and cavity. Note the core of the flux rope features a strong Stokes V signal of $\sim 1\text{--}7\%$ over a wide range of frequencies from 1–20 GHz.

Despite the potential of radio observations for deriving the detailed morphology of coronal cavities (both on the limb and against the disk) and accurately mapping B_{LOS} , **current radio facilities do not have the adequate imaging fidelity, dynamic range, and polarization purity necessary to make such measurements**. The figure on the cover page shows one of the best examples of multi-frequency radio images of a coronal cavity obtained by the Expanded Owens Valley Solar Array (EOVSA), a key pathfinder instrument for demonstrating these techniques. At low frequencies (e.g., 1.4 GHz), the filament-cavity system features a dark cavity with a bright rim.

This is because the optical depth in the low-density cavity is small compared to its rim. At higher frequencies (e.g., 13.9 GHz), however, the optically thick emission from the cooler but much denser filament starts to dominate the emission. These multi-frequency images demonstrate the feasibility of imaging the filament-cavity systems at radio wavelengths and, more importantly, the potential of using spectral analysis to derive the plasma parameters. However, owing to the small number of baselines from EOVSA’s 13 antennas, these images can only be made with several hours of integration by taking advantage of Earth’s rotation to improve the u - v coverage. Thus, crucial details of the *dynamic evolution* of the coronal cavity structures are not recovered. Additionally, owing to its limited spatial resolution, image fidelity, and dynamic range, measuring the Stokes-V signal down to the required detection level of a few percent is likely out of reach for EOVSA.

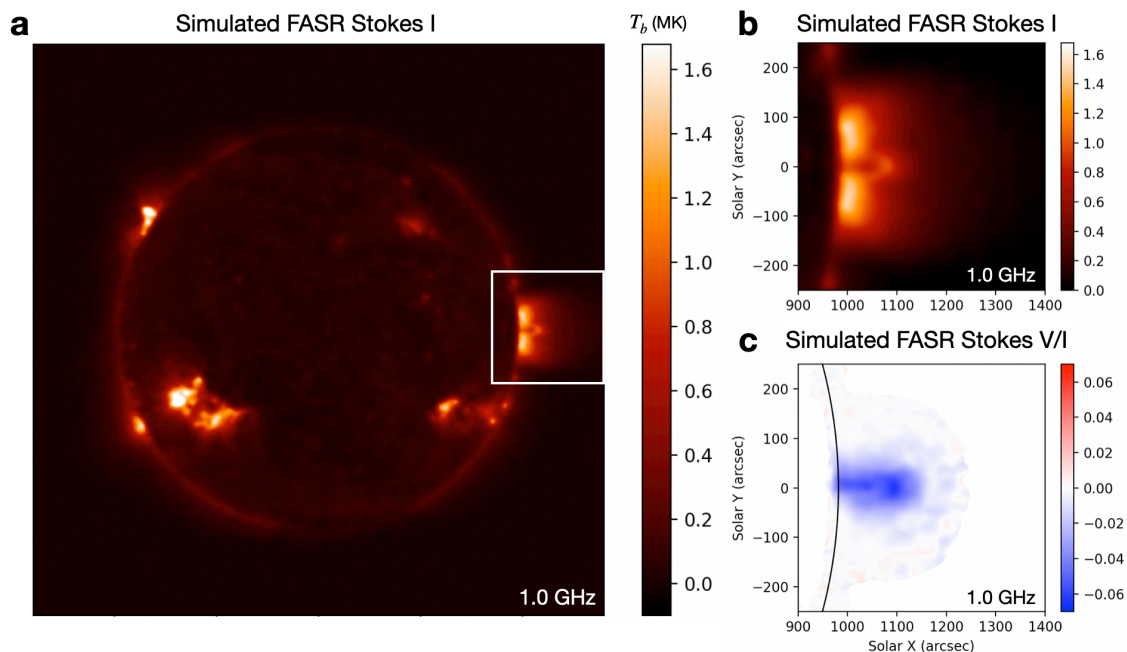


Figure 2: Simulated snapshot (1-s cadence) Stokes I and V images by an example FASR array configuration that consists of 200 2-m-diameter antennas. (a) Simulated full-disk image at 1 GHz. (b) and (c) Enlarged view of the Stokes I and V/I images of the coronal cavity region (white box in (a)). The latter is simulated from an input emission model calculated from the 3D MHD model shown in Fig. 1. The angular resolution of the array is $\sim 20''/\text{GHz}$. See text for details.

To fully exploit the potential of these radio diagnostics to study CME precursors, a radio array with a large number of antenna elements (of order 100) and accurate spectropolarimetry capabilities over a frequency range of ~ 0.5 – 20 GHz is required. With the >2 orders of magnitude increase in the number of baselines sampling the u - v domain compared to, e.g., EOVSA, the instrument will provide dramatically improved image fidelity and dynamic range. Such a superior imaging capability would allow all features with different angular scales and brightness across the full-Sun disk to be faithfully recovered. Fig. 2 shows simulated snapshot (1-s cadence) imaging results based on an example 200-element log-spiral array configuration (see Fig. 3 in Chen et al. 2022a for plots of the array configuration and performance metrics). In order to best emulate the actual observational conditions, the input “sky model” is made from the synthetic radio emission maps calculated from the 3D MHD coronal cavity model, as shown in Fig. 1, combined with a synthetic full-disk radio

map. The latter is constructed by calculating the thermal free-free radio emission using the differential emission measure map derived from multi-band SDO/AIA EUV images (Fleishman et al. 2021). This sky model is then “observed” with the model array configuration to produce complex visibilities using CASA’s `simobserve` task, and is then subsequently Fourier transformed and deconvolved using the multi-scale CLEAN algorithm (Cornwell 2008). Random noise (due to the instrument’s system temperature and residual gain errors after calibration) is introduced in the simulation to best replicate the actual observations.

Contrasting the “ground truth” shown in Fig. 1 with the simulated observations, it is evident that crucial details of the cavity brightness, morphology, and Stokes-V signatures are faithfully reproduced. Therefore, with the added broadband multi-frequency capability for performing spatially resolved spectral analysis (based on spectra similar to those in Fig. 1(g) and (h)), **such a next-generation instrument is expected to make a giant leap forward in constructing the key parameters of coronal cavities, including the elusive measurements of the strength, spatial distribution, and short-time-scale evolution of the LOS coronal magnetic field.** We emphasize that, although the discussion above focuses on coronal cavities that are long-lived structures typically observed in quiet Sun regions, with the second-scale snapshot imaging spectropolarimetry capability, **similar techniques can be applied to fast-evolving, flux-rope-hosting structures in active regions.** These active region flux rope structures, which can lead to major eruptive flare events and fast CMEs, are expected to yield more significant radio signatures because they are hotter, denser, and bears a stronger magnetic field.

3 Radio Observations of CMEs and CME-driven Shocks

When CMEs erupt, in addition to the radio emission from the ejected filaments and CME bubbles (e.g., Huang et al. 2019), energetic electrons accelerated or trapped by the CMEs or CME-driven shocks also emit a variety of nonthermal radio emissions.

3.1 Type II Radio Bursts

The most common radio signature of a fast CME is a type II radio burst, coherent plasma radiation produced by the CME-driven super-Alfvénic shock propagating in the corona and sometimes well out into the interplanetary medium. Type IIs are recognized by their characteristic slow-drift signature in dynamic spectra and have been used to constrain the density of the medium and the shock speed. They have been imaged at discrete frequencies in past years (e.g., Bain et al. 2012) but their relation to the underlying CME driver has been murky. In more recent years, instruments like the general-purpose LOFAR and the MWA have produced multi-frequency imaging of type IIs (Morosan et al. 2019). Determining the relationship between type II radio bursts and the shock driver is a key science goal of solar-dedicated imaging arrays being commissioned at long wavelengths, which include Owens Valley Long Wavelength Array (OVRO-LWA, 20-88 MHz; Chhabra et al. 2021) and the SunRISE mission (Kasper et al. 2022), which will use a space-based interferometric array covering 0.1–25 MHz. However, **tracking the initiation and development of type II radio bursts requires continuous coverage from the low corona to the middle corona.** Under typical coronal conditions, this translates to a frequency range from ~ 500 MHz down to < 20 MHz. As reviewed by Chen et al. (2022b), currently **there is no solar-dedicated radio instrument available that provides broadband dynamic imaging spectroscopy over this frequency range, although LOFAR, the MWA, and OVRO-LWA partially address the need.**

3.2 Radio CMEs

Faint radio emissions that closely resemble their white light CME counterparts are dubbed “radio CMEs” because of their similar appearance (see a recent review by [Vourlidas et al. 2020](#)). The emission mechanism is believed to be synchrotron emission which, when imaged spectroscopically, can be used to map the evolving CME magnetic field strength (and possibly direction, if polarimetry is available), non-thermal electron distribution, and the thermal electron number density (see, e.g. [Bastian et al. 2001](#)). It should be noted that the same plasma producing white light CMEs in the middle to high corona also emits *thermal* free-free radiation. This is usually difficult to detect due to low surface brightness (see discussion by [Bastian & Gary 1997](#)), although detections have been reported in the literature ([Gopalswamy & Kundu 1993](#); [Ramesh et al. 2021](#)).

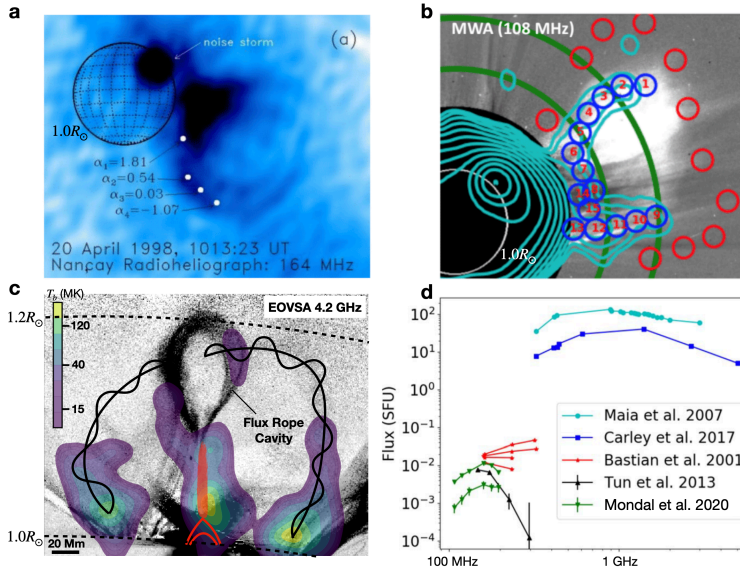


Figure 3: Examples of “radio CME” observations by the Nançay Radioheliograph ([Bastian et al. 2001](#)) (a) and the MWA ([Mondal et al. 2020](#)) (b) in the middle corona at metric wavelengths. (c) A high-frequency counterpart of radio CME observed by EOVSA in the low corona at ~ 4.2 GHz ([Chen et al. 2020](#)). (d) Spectra of some reported radio CME events ([Mondal et al. 2020](#)).

Since the original detections made by the Nançay Radioheliograph operating between 150–450 MHz (see Fig. 3(a) for an example), few radio CMEs have been reported. Recently, emission surrounding a flux rope cavity, which could be considered a radio CME at its initiation phase, was detected with EOVSA at ~ 4.2 GHz in the low corona ($\sim 1.2R_{\odot}$; Fig. 3(c)). More recently, a faint radio CME event was observed from 80–240 MHz by the MWA (Fig. 3(b); [Mondal et al. 2020](#)). The event shared a similar morphology to those reported earlier but was associated with a much slower (< 500 km s^{-1}) and fainter (of order 0.001–0.01 sfu) CME. Such an unprecedented detection was made possible thanks to MWA’s ability to perform highly sensitive, high dynamic range imaging with its 128 antenna elements. With spatially resolved spectral analysis, a magnetic field strength of ~ 10 G was derived at the outer “shell” of the CME bubble. In addition, the number density and power-law index of the nonthermal electron distribution were also constrained.

This outstanding example, obtained by a state-of-the-art general-purpose facility (i.e. proposal driven), provides a glimpse of the unique power of radio observations for constraining the magnetic field configuration and nonthermal electron distribution of erupting CMEs with a variety of speeds and strengths. **These diagnostics, however, call for routine solar-dedicated observations with high sensitivity and high dynamic range imaging spectroscopy. In addition, to trace and measure the radio CMEs from their initiation in the low corona to their evolution in the middle corona, a continuous frequency coverage over 10s of MHz to a few GHz is required.**

4 Observing the System: Findings and Recommendations

To conclude, radio observations can be used in a unique and wholly new manner to constrain the formation, evolution, destabilization, and eruption of CMEs and CME progenitors. Especially powerful will be joint optical/IR/(E)UV and radio observations of coronal cavities as *CME precursors* and their destabilization into nascent CMEs, with multi-wavelength coronal spectropolarimetry yielding sensitivity to different parts of the emitting coronal plasma through a variety of physical mechanisms (Gibson et al. 2021; see e.g., Table 1), leading to the robust reconstruction of their 3D coronal magnetic field. Equally important are the *unique* diagnostics offered by radio observations on the magnetic field and nonthermal electron distribution of *erupting CMEs and the associated shocks* as they lift off and propagate into the upper corona. To briefly summarize the discussion above:

- CME precursors (Sec. 2): Radio (this paper) and O/IR (white paper by Gibson et al. 2022) observations from the ground and UV observations from space (white paper by Casini et al. 2022) offer powerful and complementary diagnostics of the plasma environment in and around coronal cavities. Radio observations of thermal free-free emission and polarimetry will yield the line-of-sight component of the magnetic field of coronal cavities and flux-rope-hosting structures in both quiescent and active regions. Unlike optical/IR observations, which for this goal can only be taken above the limb, radio observations can be made of coronal cavities, filament channels, and sigmoids on the disk.
- Erupting CMEs and CME-driven shocks (Sec. 3): The erupting magnetic flux ropes/CMEs can be imaged at radio wavelengths if it has significant numbers of energetic electrons entrained in their magnetic field. As the eruption evolves into an eruptive flare, the magnetic field and the electron distribution function can be measured as a function of time and space—in the reconnecting magnetic loops/current sheet (white paper by Chen et al. 2022a) and the erupting CME themselves (this paper). Ground-based radio observations can make these measurements dynamically across the evolving CME out to several solar radii. Faraday Rotation (FR) measurements provide additional constraints on the CME density and magnetic field (Kooi et al. 2022). Any type II radio burst, tracing a shock that accompanies the CME, may also be imaged simultaneously.

The above elements require radio coverage from a few 10s of MHz to 20 GHz in order to observe them as a coupled system. To make transformative advances in making new and unique measurements discussed above, a solar-dedicated radio facility with a large number of elements (of order 100) is required to obtain broadband radio imaging spectropolarimetry with high image fidelity, dynamic range, angular resolution, and sensitivity. In the past decade, significant investments have been made in ground-based low-frequency arrays at frequencies $\lesssim 0.2$ GHz with the operation of LOFAR, MWA, and the solar-dedicated OVRO-LWA (see Fig. 5 of Chen et al. 2022b for a synopsis). Therefore, in the coming decade, we suggest the focus should be placed in the ~ 0.2 –20 GHz range.

The *Frequency Agile Solar Radiotelescope* (FASR) is a concept for realizing such high sensitivity, image fidelity, and dynamic range imaging spectropolarimetry observations in an ultra-wide frequency range of ~ 0.2 –20 GHz. We refer readers to Gary et al. (2022) and references therein for a more detailed discussion of the instrument and a broad range of breakthrough science it is expected to achieve.

References

- Bain, H. M., Krucker, S., Glesener, L., et al. 2012, *Radio Imaging of Shock-accelerated Electrons Associated with an Erupting Plasmoid on 2010 November 3*, ApJ, 750, 44, [10.1088/0004-637X/750/1/44](https://doi.org/10.1088/0004-637X/750/1/44)
- Bak-Stęślicka, U., Gibson, S. E., Fan, Y., et al. 2013, *The Magnetic Structure of Solar Prominence Cavities: New Observational Signature Revealed by Coronal Magnetometry*, ApJ, 770, L28, [10.1088/2041-8205/770/2/L28](https://doi.org/10.1088/2041-8205/770/2/L28)
- Bastian, T. S., & Gary, D. E. 1997, *On the feasibility of imaging coronal mass ejections at radio wavelengths*, J. Geophys. Res., 102, 14031, [10.1029/97JA00483](https://doi.org/10.1029/97JA00483)
- Bastian, T. S., Pick, M., Kerdraon, A., et al. 2001, *The Coronal Mass Ejection of 1998 April 20: Direct Imaging at Radio Wavelengths*, ApJ, 558, L65, [10.1086/323421](https://doi.org/10.1086/323421)
- Carley, E. P., Vilmer, N., & Vourlidas, A. 2020, *Radio observations of coronal mass ejection initiation and development in the low solar corona*, Frontiers in Astronomy and Space Sciences, 7, 79, [10.3389/fspas.2020.551558](https://doi.org/10.3389/fspas.2020.551558)
- Casini, R., Gibson, S., Newmark, J., et al. 2022, *Solar Coronal Polarization Diagnostics with H I Ly- α* , White Paper Submitted to the Decadal Survey for Solar and Space Physics
- Casini, R., White, S. M., & Judge, P. G. 2017, *Magnetic Diagnostics of the Solar Corona: Synthesizing Optical and Radio Techniques*, Space Sci. Rev., 210, 145, [10.1007/s11214-017-0400-6](https://doi.org/10.1007/s11214-017-0400-6)
- Chen, B., Yu, S., Reeves, K. K., et al. 2020, *Microwave Spectral Imaging of an Erupting Magnetic Flux Rope: Implications for the Standard Solar Flare Model in Three Dimensions*, ApJ, 895, L50, [10.3847/2041-8213/ab901a](https://doi.org/10.3847/2041-8213/ab901a)
- Chen, B., Gary, D., Fleishman, G., et al. 2022a, *Quantifying Solar Flare Energy Release: New Frontiers with a Next-Generation Solar Radio Facility*, White Paper Submitted to the Decadal Survey for Solar and Space Physics
- Chen, B., Kooi, J., Wexler, D., et al. 2022b, *Radio Studies of the Middle Corona: Current State and New Prospects in the Next Decade*, White Paper Submitted to the Decadal Survey for Solar and Space Physics
- Chhabra, S., Gary, D. E., Hallinan, G., et al. 2021, *Imaging Spectroscopy of CME-associated Solar Radio Bursts Using OVRO-LWA*, ApJ, 906, 132, [10.3847/1538-4357/abc94b](https://doi.org/10.3847/1538-4357/abc94b)
- Cornwell, T. J. 2008, *Multiscale CLEAN Deconvolution of Radio Synthesis Images*, IEEE Journal of Selected Topics in Signal Processing, 2, 793, [10.1109/JSTSP.2008.2006388](https://doi.org/10.1109/JSTSP.2008.2006388)
- Fan, Y., & Liu, T. 2019, *MHD simulation of prominence-cavity system*, Frontiers in Astronomy and Space Sciences, 6, 27, [10.3389/fspas.2019.00027](https://doi.org/10.3389/fspas.2019.00027)

- Fleishman, G. D., Kuznetsov, A. A., & Landi, E. 2021, *Gyroresonance and Free-Free Radio Emissions from Multithermal Multicomponent Plasma*, ApJ, 914, 52, [10.3847/1538-4357/abf92c](https://doi.org/10.3847/1538-4357/abf92c)
- Gary, D., Chen, B., Fleishman, G., et al. 2022, *Frequency Agile Solar Radiotelescope: A Next-Generation Radio Telescope for Solar Physics and Space Weather*, White Paper Submitted to the Decadal Survey for Solar and Space Physics
- Gibson, S., Bak-Steslicka, Urszula, Casini, R., et al. 2022, *Coronal Polarimetry: Determining the Magnetic Origins of Coronal Mass Ejections*, White Paper Submitted to the Decadal Survey for Solar and Space Physics
- Gibson, S., Kucera, T., White, S., et al. 2016, *FORWARD: A toolset for multiwavelength coronal magnetometry*, Frontiers in Astronomy and Space Sciences, 3, 8, [10.3389/fspas.2016.00008](https://doi.org/10.3389/fspas.2016.00008)
- Gibson, S., Malanushenko, A., de Toma, G., et al. 2021, *Untangling the Global Coronal Magnetic Field with Multiwavelength Observations*, White Paper Submitted to Helio2050. <https://www.hou.usra.edu/meetings/helio2050/pdf/4062.pdf>
- Gibson, S. E., Foster, D., Burkepile, J., et al. 2006, *The Calm before the Storm: The Link between Quiescent Cavities and Coronal Mass Ejections*, ApJ, 641, 590, [10.1086/500446](https://doi.org/10.1086/500446)
- Gopalswamy, N., & Kundu, M. R. 1993, *Thermal and nonthermal emissions during a coronal mass ejection*, Sol. Phys., 143, 327, [10.1007/BF00646491](https://doi.org/10.1007/BF00646491)
- Huang, J., Tan, B., Masuda, S., et al. 2019, *Localized Microwave and EUV Bright Structures in an Eruptive Prominence*, ApJ, 874, 176, [10.3847/1538-4357/ab0e80](https://doi.org/10.3847/1538-4357/ab0e80)
- Kasper, J., Lazio, T. J. W., Romero-Wolf, A., et al. 2022, in 2022 IEEE Aerospace Conference (AERO) (IEEE), [10.1109/aero53065.2022.9843607](https://doi.org/10.1109/aero53065.2022.9843607)
- Kooi, J., Wexler, D., Jensen, E., et al. 2022, *How to Advance Studies of Coronal Faraday Rotation*, White Paper Submitted to the Decadal Survey for Solar and Space Physics
- Mondal, S., Oberoi, D., & Vourlidis, A. 2020, *Estimation of the Physical Parameters of a CME at High Coronal Heights Using Low-frequency Radio Observations*, ApJ, 893, 28, [10.3847/1538-4357/ab7fab](https://doi.org/10.3847/1538-4357/ab7fab)
- Morosan, D. E., Carley, E. P., Hayes, L. A., et al. 2019, *Multiple regions of shock-accelerated particles during a solar coronal mass ejection*, Nature Astronomy, 3, 452, [10.1038/s41550-019-0689-z](https://doi.org/10.1038/s41550-019-0689-z)
- Ramesh, R., Kumari, A., Kathiravan, C., et al. 2021, *New Results on the Direct Observations of Thermal Radio Emission from a Solar Coronal Mass Ejection*, Geophys. Res. Lett., 48, e91048, [10.1029/2020GL091048](https://doi.org/10.1029/2020GL091048)
- Reeves, K. K., Gibson, S. E., Kucera, T. A., et al. 2012, *Thermal Properties of a Solar Coronal Cavity Observed with the X-Ray Telescope on Hinode*, ApJ, 746, 146, [10.1088/0004-637X/746/2/146](https://doi.org/10.1088/0004-637X/746/2/146)

- Schmit, D. J., & Gibson, S. E. 2011, *Forward Modeling Cavity Density: A Multi-instrument Diagnostic*, ApJ, 733, 1, [10.1088/0004-637X/733/1/1](https://doi.org/10.1088/0004-637X/733/1/1)
- Tomczyk, S., Burkepile, J., Casini, R., et al. 2022, *COSMO: The COronal Solar Magnetism Observatory*, White Paper Submitted to the Decadal Survey for Solar and Space Physics
- Vourlidas, A., Carley, E. P., & Vilmer, N. 2020, *Radio Observations of Coronal Mass Ejections: Space Weather Aspects*, Frontiers in Astronomy and Space Sciences, 7, 43, [10.3389/fspas.2020.00043](https://doi.org/10.3389/fspas.2020.00043)